

High-Energy Electron Scattering and Nuclear Structure Determinations. III. Carbon-12 Nucleus*†

JEROME H. FREGEAU‡ AND ROBERT HOFSTADTER

Department of Physics and W. W. Hansen Laboratories of Physics, Stanford University, Stanford, California

(Received May 10, 1955)

The elastic scattering peak in carbon-12 is accompanied by a number of additional peaks corresponding to inelastic scattering of electrons from the various excited levels of the carbon nucleus. Three levels have been investigated by this method and correspond to the three known states at 4.43 Mev, 7.68 Mev, and 9.61 Mev. Angular distributions of the inelastically-scattered electrons have been obtained as well as the angular distribution of the elastically-scattered electrons. The angular distributions of the inelastic peaks fall off less steeply with angle than the elastic peak. By comparing the scattering from carbon with scattering from the proton, and using the theoretical value of the cross section of electrons scattered from the proton, it is possible to obtain "absolute" values for the elastic and inelastic scattering cross sections. From the elastic-scattering curve, information about the size and charge distribution in the carbon-12 nucleus may be derived. The charge distribution lies halfway between a Gaussian and a uniform model. The root mean square radius of the resultant charge distribution is $(2.40 \pm 0.25) \times 10^{-13}$ cm.

I. INTRODUCTION

THE study of electron scattering at high energies (100–200 Mev) has led to certain conclusions about the electromagnetic size of nuclei and to interesting information about the variation of charge density near the surface of the nucleus.^{1–4} Recently it has been shown⁵ that electrons may be scattered from nuclei inelastically as well as elastically and that sharp peaks corresponding to nuclear levels accompany the elastic peak. We have thought it worthwhile to make a more intensive study of such inelastic and elastic structure at various angles of scattering in a light, well-known nucleus. In this way phenomenological information about the behavior of the inelastic scattering might be obtained and could assist possible theoretical interpretations of the experimental data.^{6,7} Carbon-12 seemed an ideal nucleus in view of the large amount of information available in the literature on its excited levels. Furthermore, there is considerable interest in the nature of the second level at 7.68 Mev both in regard to the type of transition (probably $0^+ \rightarrow 0^+$) and to its influence in the production of stellar energy.

II. APPARATUS

The apparatus used in these studies has been described in two previous publications.^{1,2} Several improvements have been made, as follows:

* The research reported in this document was supported jointly by the Office of Naval Research and the U. S. Atomic Energy Commission, and by the U. S. Air Force through the Office of Scientific Research of the Air Research and Development Command.

† Aided by a grant from the Research Corporation.

‡ International Business Machines Fellow for the year 1954–55.

¹ Hofstadter, Fechter, and McIntyre, *Phys. Rev.* **91**, 422 (1953); **92**, 978 (1953).

² Hofstadter, Hahn, Knudsen, and McIntyre, *Phys. Rev.* **95**, 512 (1954).

³ D. G. Ravenhall and D. R. Yennie, *Phys. Rev.* **96**, 239 (1954).

⁴ D. L. Hill and K. Ford (private communication).

⁵ McIntyre, Hahn, and Hofstadter, *Phys. Rev.* **94**, 1084 (1954).

⁶ L. I. Schiff, *Phys. Rev.* **96**, 765 (1954); *Phys. Rev.* **98**, 1281 (1955).

⁷ C. J. Mullin and E. Guth, *Phys. Rev.* **98**, 277(A) (1955).

(1) The slits at the entrance and exit of the magnet are now remotely controlled.

(2) The lining up of the beam has been greatly facilitated by the use of a luminescent crystal placed on the axis of the scattering system and viewed by a system of mirror (or mirrors) and telescope. The latter is placed in the laboratory room where the counting is carried on. Thallium-activated cesium bromide has proved very successful in this application and exhibits a bright green glow which can be seen even at fifty feet without the telescope. The crystal darkens surprisingly little under intense electron bombardment. Thallium-activated potassium iodide has also been used but is not as useful as the cesium bromide. The viewing system was suggested and perfected by A. W. Knudsen.

(3) A device has been installed to calibrate the photomultiplier-Čerenkov counter system. The Čerenkov counter is used as the detector of the analyzed electrons. A radioactive source (actually the uranium slit-jaw at the exit of the spectrometer) provides gamma rays which impinge on an anthracene crystal. The anthracene crystal is situated on a movable plate which slides the crystal either in front of the entrance to the Čerenkov counter or removes it and substitutes a thin aluminum window through which the scattered electrons pass into the Čerenkov counter after emerging from the magnetic analyzer. Thus, when it is desired to calibrate the counter system, the anthracene crystal is moved in front of the Čerenkov counter (now acting as a light pipe) and the number of counts is recorded for a given interval of time. After checking, the anthracene is moved out of the way by remote control and the system is ready to receive electrons through the thin window. Under the optical conditions prevailing, the anthracene pulses are quite similar in size to the Čerenkov pulses from the high-energy electrons. The details of this calibration scheme were worked out by E. E. Chambers and B. Chambers.

(4) A secondary emitter has been installed for beam

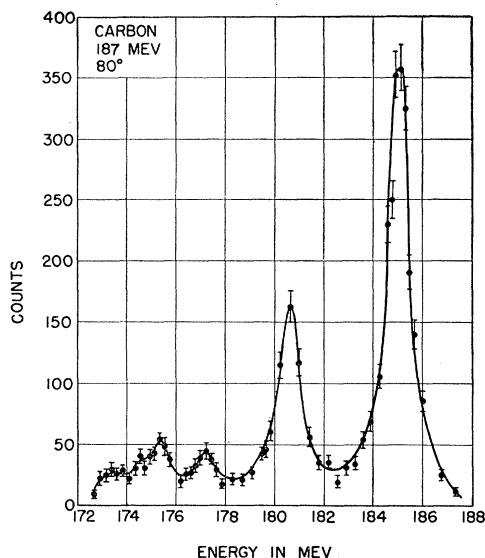


FIG. 1. The elastic and inelastic peaks at 187 Mev in carbon at a scattering angle of 80° .

monitoring purposes. Such a beam monitor has been described recently.⁸

III. PROCEDURE

Our general procedure has been to make a run at a given angular setting of the magnet during which the number of scattered electrons is measured as a function of the current in the magnet. Since the calibration curve of magnetic field *vs* magnetizing current is known, the number of scattered electrons may then be plotted as a function of their energy. At any angle the elastic and inelastic features are thus measured during the same run. At some later time the elastic peaks are related to each other by measuring in a single run all the elastic peaks alone at the various angles previously studied. Since the ratio of inelastic to elastic peaks is known from the previous runs, all the inelastic peaks can be related to each other.

In the course of taking the elastic runs in carbon, the elastic peaks of hydrogen (or sometimes a single peak) are also observed and measured. The protons in polyethylene (CH_2)⁹ are used for this purpose. By carrying out the comparison runs of the proton peaks *vs* the carbon elastic peaks, the carbon peaks may be normalized. If the theoretical values of the proton cross section are used, the ratio of the areas of the carbon peaks to the proton peaks times the theoretical cross section for the proton gives the "absolute" cross section of the elastic scattering from carbon. Similarly the inelastic cross section may be derived absolutely by reference to electron scattering from the proton.

⁸ G. W. Tautfest and H. R. Fechter, *Phys. Rev.* **96**, 35 (1954); *Rev. Sci. Instr.* **26**, 229 (1955).

⁹ The number of protons is assumed to be exactly twice the number of carbon nuclei. This figure is probably accurate to a few tenths of a percent or better.

In Figs. 1 and 2 we show two typical runs of the elastic and inelastic peaks at a given angle and at a given energy (187 Mev). In Fig. 3 we give a set of elastic peaks at a given incident energy at the various angles studied. Also given in Fig. 3 is a comparison proton peak which has been used for normalization of the carbon data. It will be noticed that the carbon peaks shift slightly in energy as the angle of scattering is changed. This effect has been noticed previously¹ and is due to a combination of recoil of the carbon nucleus and energy loss in the scattering layer. In these experiments the target plane was rotated so that the normal to the target always bisected the angle of scattering. The thickness of the target in the beam was therefore variable and appropriate correction was made in reduction of the data. The large shift in energy of the proton peak may also be noted. This shift has also been observed previously.¹ In all the runs the angular width accepted by the spectrometer was $\pm 1.3^\circ$.

In these experiments the exit slit was maintained at constant width during all the runs. Thus the slit selected a fixed percentage of the particular energy at which the spectrometer was set. Consequently, the absolute energy interval accepted by the exit slit varies since the peaks appear at slightly different energies at the various angles. Curves taken with a wide (energy) slit give proportionately more counts in the peak than those curves taken with a narrow (energy) slit. Therefore a correction has to be applied to the raw data. In the case of the carbon peaks the correction is less than one percent over the range of angles studied. In the case of hydrogen, however, the largest correction amounts to approximately seven percent.

The inelastic peaks appear to "ride" on the bremsstrahlung tail of the elastic peak. This tail falls off approximately as the reciprocal of the energy interval between a given energy and that of the elastic peak. A subtraction of the background in the tail is required in order to obtain the ordinate of the inelastic peak. In most cases it has not proved more accurate to use the

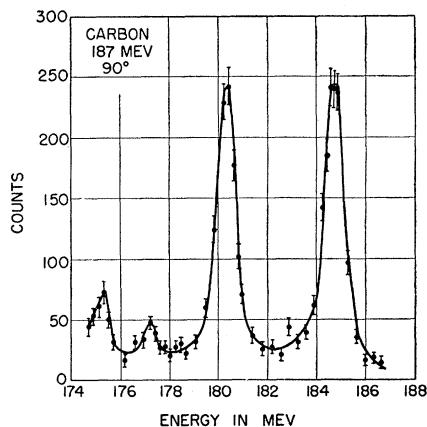


FIG. 2. The elastic and inelastic peaks at 187 Mev in carbon at a scattering angle of 90° .

$1/E$ dependence in estimating the bremsstrahlung tail, than sketching in the background by inspection of the regions higher and lower in energy than the inelastic peak and continuing this background under the peak. The latter procedure has been used in estimating the inelastic scattering.

IV. RESULTS

A. Inelastic Data

Data have been taken at three energies: 187 Mev, 150 Mev, and 80 Mev. The data at 187 Mev are the most extensive. At 80 Mev very few data have been obtained because of the difficulty in seeing the inelastic peaks over the bremsstrahlung tails of the elastic peaks.

The 187-Mev data are summarized in Fig. 4. This figure shows the angular distributions of the elastic scattering (Curve A) and the distributions of the inelastic scatterings corresponding to the three inelastic levels (Curve B, 4.43 Mev; Curve C, 7.68 Mev; and Curve D, 9.61 Mev). Table I also gives a summary of the data shown in Fig. 4. The cross sections are given in absolute units because of the normalization made in terms of the theoretical cross section of electron scattering from the proton.

A word of explanation is necessary here. In using the theoretical cross section for hydrogen, the formula of Rosenbluth¹⁰ has been used. We have employed his point-charge and point-magnetic moment (anomalous value) approximation, except as modified slightly by results obtained recently in this laboratory.¹¹ Finally the radiative correction of Schwinger¹² has been applied to the hydrogen data. The latter correction amounts to a decrease of approximately 15 percent at 187 Mev for the 3-Mev band width of the hydrogen peak used in our normalization. For example, the hydrogen cross

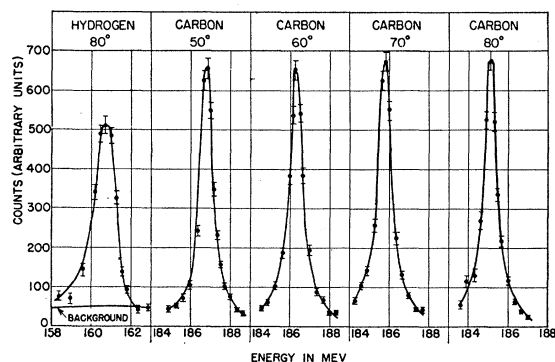


FIG. 3. The elastic peaks in carbon at an incident energy of 187 Mev and at various angles of scattering. The elastic scattering curve for the protons in polyethylene is also shown at a scattering angle of 80°. The greater half-width of the proton peak is due principally to recoil effects. The background under the hydrogen peak is taken from another run.

¹⁰ M. Rosenbluth, Phys. Rev. **79**, 615 (1950).

¹¹ R. Hofstadter and R. McAllister, Phys. Rev. **98**, 217 (1955).

¹² J. Schwinger, Phys. Rev. **75**, 898 (1949); **76**, 790 (1949).

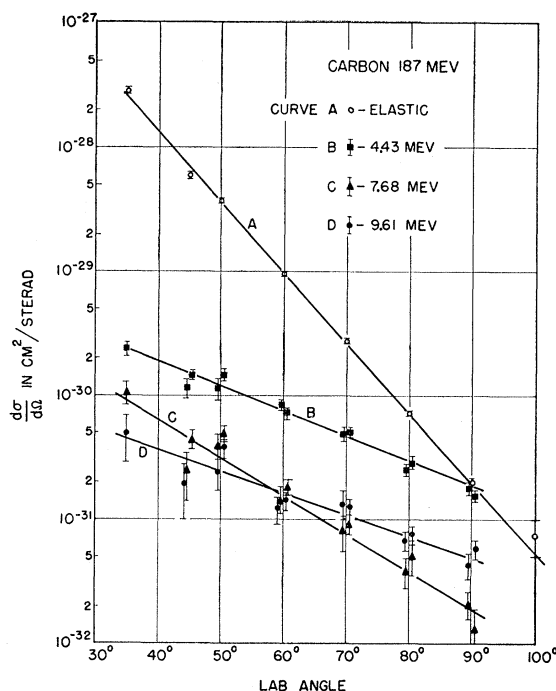


FIG. 4. The angular distributions of the elastic and inelastic peaks at 187 Mev in carbon. The absolute cross sections have been obtained by the proton-normalization method discussed in the text.

TABLE I. Cross section of elastic and inelastic scattering peaks in microbarns per steradian for various angles at an incident energy of 187 Mev. The radiative correction is included.

Lab angle	Elastic	4.43 Mev	7.68 Mev	9.61 Mev
35°	283±14	2.35±0.28	1.05±0.22	0.49±0.20
45°	68.7±3.5	1.13±0.19	0.24±0.10	0.19±0.09
50°	36.3±1.1	1.41±0.11	0.44±0.08	0.24±0.07
		1.46±0.16	0.49±0.07	0.39±0.08
60°	9.42±0.38	0.828±0.083	0.144±0.035	0.121±0.030
		0.715±0.086	0.180±0.027	0.141±0.024
70°	2.72±0.11	0.484±0.063	0.080±0.025	0.133±0.035
		0.500±0.050	0.092±0.017	0.127±0.019
80°	0.714±0.028	0.251±0.025	0.038±0.010	0.068±0.012
		0.286±0.034	0.051±0.016	0.075±0.013
90°	0.199±0.014	0.179±0.021	0.021±0.005	0.043±0.010
		0.157±0.017	0.013±0.006	0.058±0.010

section at 50° is 3.6×10^{-30} cm²/sterad and with the radiative correction it becomes 3.0×10^{-30} cm²/sterad. This means that the carbon cross sections computed from these figures include a radiative correction.

Data similar to those in Fig. 4 are presented in Fig. 5 for the case of 150 Mev. Table II gives the corresponding summary of data. Figure 6 shows a typical run taken at 90° at this energy. One notes the strong contrast of these data with those shown in Fig. 2 which are also taken at 90° but at the higher energy (187 Mev). One observes the clear effect of the diminution in the elastic peak at the higher energy which makes the inelastic peak appear more prominent at the higher

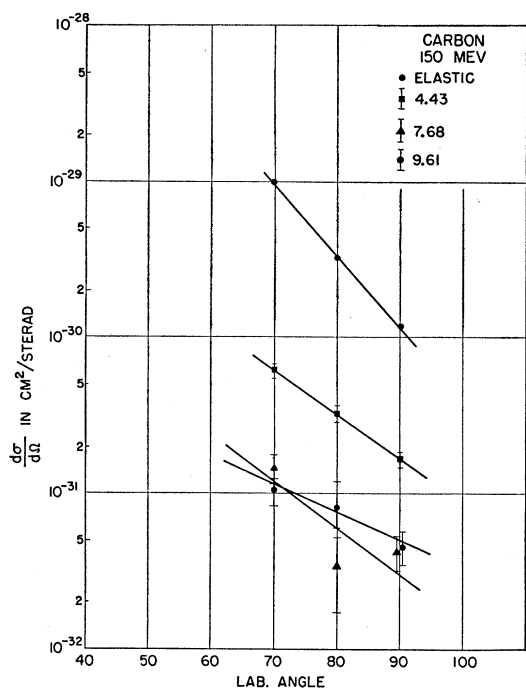


FIG. 5. The angular distributions in carbon at 150 Mev of the elastic and inelastic peaks. The absolute cross sections have been obtained by the proton-normalization method discussed in the text.

energy. In fact, it is only because of the large reduction in elastic scattering¹ due to the finite nuclear size that the inelastic peaks have become evident.⁵ The bremsstrahlung tail goes down in proportion to the elastic scattering and the inelastic peaks may thus be seen more easily on the lower backgrounds at higher energies. The data at 187 Mev and at 150 Mev show that the

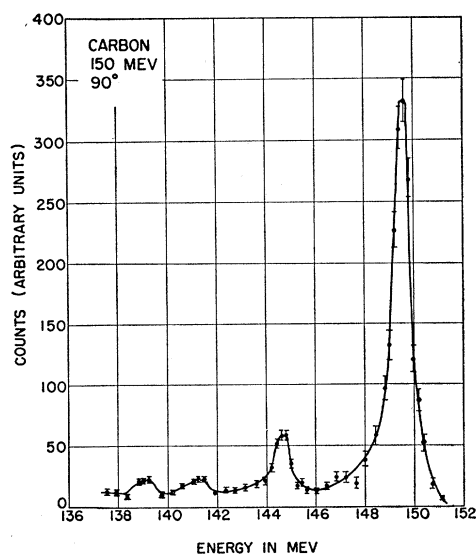


FIG. 6. The elastic and inelastic peaks at 150 Mev in carbon at a scattering angle of 90°. This figure should be compared with Fig. 2.

angular distribution of the inelastic scattering is less steep than the corresponding data for the elastic scattering. This appears to be a general conclusion for all the levels thus far studied in carbon. One also notices that the angular distributions of the 4.43-Mev and 9.61-Mev peaks appear to be similar to each other and both are different from that of the 7.68-Mev peak. The two subsidiary peaks 10.80 Mev and 11.75 Mev (combined with 11.1 Mev) in the various figures seem to vary in roughly, but not exactly, the same way as the 9.61-Mev peak, but the resolution of these peaks and the small number of counts recorded for them do not permit any strict conclusions to be drawn.

In view of the assignment 2^+ for the 4.43-Mev state and the similarity of angular distributions of the 4.43- and 9.61-Mev peaks, we are tempted to make the assignment of 2^+ to the 9.61-Mev state. The interpretation of the 7.68-Mev transition as $0^+ \rightarrow 0^+$ is not inconsistent with the differences observed between the angular distributions of the 7.68- and 4.43-Mev peaks.

The strong dependence on energy of the "visibility" of the inelastic peaks above the bremsstrahlung tail has prompted us to examine the inelastic and elastic

TABLE II. Cross section of elastic and inelastic scattering peaks in microbarns per steradian for various angles at an incident energy of 150 Mev. The radiative correction is included.

Lab. angle	Elastic	4.43 Mev	7.68 Mev	9.61 Mev
70°	9.90 ± 0.40	0.618 ± 0.068	0.150 ± 0.026	0.104 ± 0.021
80°	3.23 ± 0.13	0.323 ± 0.042	0.034 ± 0.017	0.081 ± 0.021
90°	1.17 ± 0.04	0.166 ± 0.018	0.042 ± 0.011	0.046 ± 0.011

scattering at 80 Mev. Figure 7 shows the corresponding data at 90° at this energy. From the data taken at the three energies one may obtain the absolute cross section for the 4.43-Mev peak at 90° as a function of the incident energy. See also Fig. 10. It may be observed that the absolute cross section at 90° is essentially constant as the energy is varied. Unfortunately for the observation of these peaks, the elastic cross section increases in a very rapid fashion because of the increasing de Broglie wavelength relative to the finite size of the carbon-12 nucleus.

The difficulty in observing the inelastic peaks above the bremsstrahlung at low values of the incident energy is matched by the difficulty in observing these peaks at small angles even at a high energy. Figure 8 shows the weak inelastic peaks at 187 Mev at small angles relative to both the elastic peak and its bremsstrahlung tail. Figures 2, 6, 7, and 8 suggest that perhaps for light nuclei the cross section for the inelastic peaks may be essentially a point charge cross section σ_p multiplied into the square of a form factor just as the elastic cross section can be represented in this way when the Born

approximation is valid (light nuclei).^{1,13-16} Here σ_p is given by

$$\sigma_p = \left(\frac{Ze^2}{2E} \right)^2 \frac{\cos^2(\theta/2)}{\sin^4(\theta/2)} \quad (1)$$

The form factor for the inelastic cross section might be expected to be a function of the momentum transfer q , where

$$q = (4\pi/\lambda) \sin(\theta/2), \quad (2)$$

or more appropriately qa , where a is a parameter having to do with the nuclear radius or size and having the dimensions of a length; qa is thus dimensionless; λ is the de Broglie wavelength of the incident electrons; and θ is the angle of scattering. [See reference 1, formulas (1) and (2) and accompanying discussion.]

To bring out such facts more clearly, the cross section

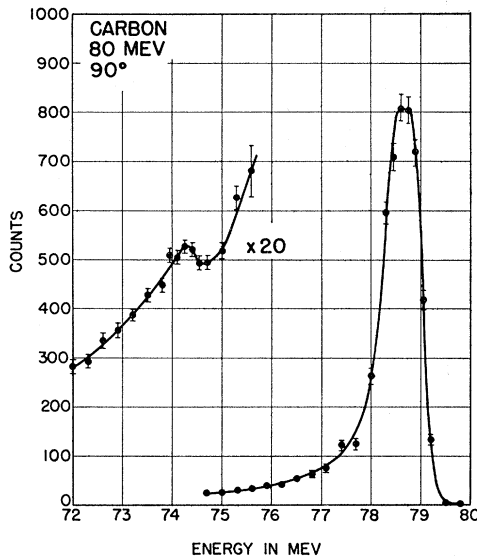


FIG. 7. The elastic and inelastic peaks at 80 Mev at a scattering angle of 90°.

for the inelastic peak at 4.43 Mev has been divided by the point charge scattering in carbon and has been plotted as a function of q in Fig. 9. The fact that a single curve is obtained strongly suggests that a form factor applies to the inelastic scattering. Ravenhall¹⁷ has employed the Born approximation and has found the type of form factor appropriate to the inelastic scattering.

It is also interesting to attempt to learn something of the origin of the inelastic peaks, i.e., to find out if the excitation of a level corresponds to a single particle excitation or to some more complicated type of nuclear

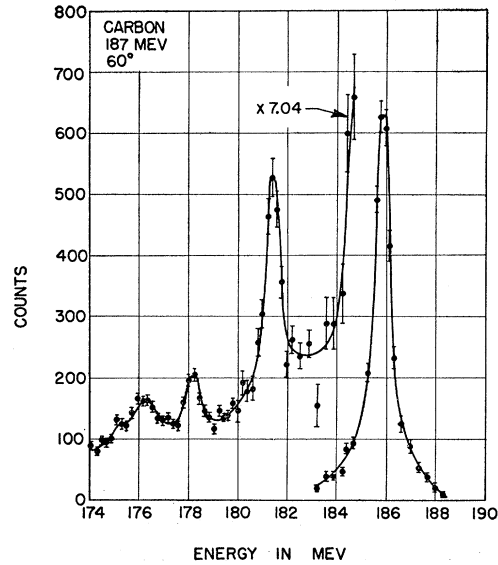


FIG. 8. The elastic and inelastic peaks at 187 Mev in carbon at a scattering angle of 60°.

excitation. In this connection it may be of potential value to compare the inelastic cross section for excitation of a particular level with the elastic cross section for electron scattering from a single proton. This ratio can be obtained from the data of Fig. 9 by multiplying the ordinate by Z^2 . A tabulation of values is given in Table III.

Finally we show in Fig. 10 the behavior of the

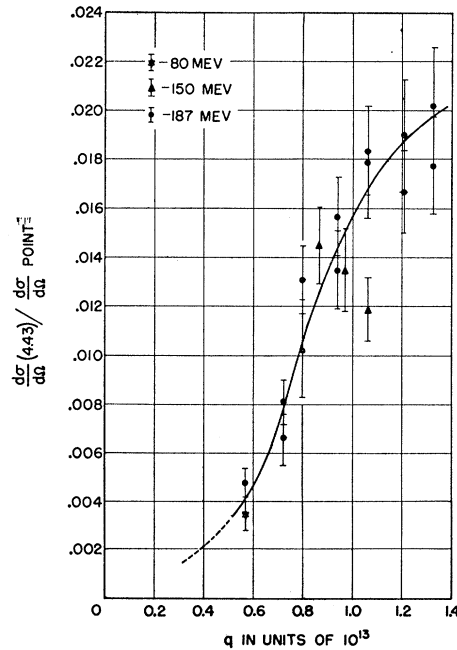


FIG. 9. The ratio of the cross section for the inelastic peak at 4.43 Mev to the point charge cross section for carbon as a function of the momentum transfer q . The black circles refer to 187 Mev, the triangles to 150 Mev and the star to 80 Mev.

¹³ E. Guth, Wien. Anzeiger Akad. Wiss. No. 24, 229 (1934).

¹⁴ M. E. Rose, Phys. Rev. **73**, 282 (1948).

¹⁵ J. H. Smith, Phys. Rev. **95**, 271 (1954).

¹⁶ L. I. Schiff, Phys. Rev. **92**, 988 (1953).

¹⁷ D. G. Ravenhall (to be published).

TABLE III. Ratio of cross section for excitation of 4.43-Mev level to point-nucleus scattering cross section for carbon.

Energy (Mev)	Lab angle	Ratio
80	90°	0.0035±0.0008
150	90°	0.0119±0.0013
150	80°	0.0135±0.0017
150	70°	0.0145±0.0016
187	90°	0.0202±0.0024
		0.0178±0.0020
187	80°	0.0167±0.0017
		0.0190±0.0023
187	70°	0.0179±0.0023
		0.0184±0.0019
187	60°	0.0157±0.0016
		0.0135±0.0016
187	50°	0.0103±0.0020
		0.0131±0.0014
187	45°	0.0066±0.0011
		0.0081±0.0010
187	35°	0.0048±0.0006

inelastic peaks at 90° as a function of energy for the three levels studied. These data indicate what may be expected in going to the lower energies available in the conventional betatron.

B. Elastic Data

Calculations made with the Born approximation are expected to be accurate to better than 5% for carbon ($Z=6$). Therefore one may attempt to fit the experimental elastic curves in carbon at 187 Mev and 150 Mev by a product of a point charge curve and the square of a form factor. The form factor may be chosen from

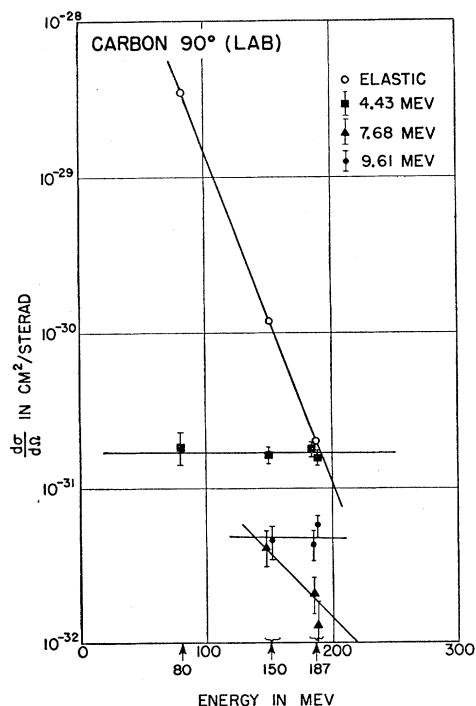


FIG. 10. The cross sections for the elastic and inelastic peaks at 90° as a function of energy.

among those appropriate to several different nuclear charge distributions. The particular charge distribution giving the best agreement with experiment will then be assumed to provide the best model for the carbon nucleus. At 187 Mev the best fit appears to lie between a Gaussian charge distribution with an rms radius of 2.47×10^{-13} cm and a uniform charge distribution with an rms radius of 2.20×10^{-13} cm. A uniform charge distribution does not appear to fit unless modified by adding a taper at the edge. A half-uniform half-Gaussian model¹ would undoubtedly provide an excellent fit to

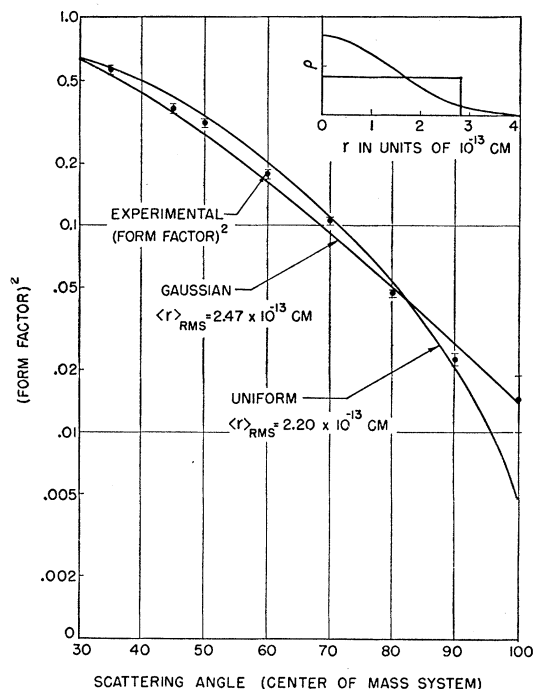


FIG. 11. This figure shows the square of the form factor plotted against scattering angle in degrees in the center-of-mass system. The square of the form factor represents the ratio of the experimental carbon cross section to the point charge cross section. The experimental points are shown in black circles, while the theoretical curves for a uniform charge distribution with rms radius of 2.20×10^{-13} cm and for a Gaussian charge distribution with rms radius of 2.47×10^{-13} cm, are given as solid lines. Neither curve fits exactly and the points lie in between the curves. This suggests a half-uniform half-Gaussian model with rms radius of approximately 2.40×10^{-13} cm. The appropriate charge distributions are shown in the upper right hand corner of the figure. The ordinate is the charge density on a linear scale.

the data and the rms radius would be close to 2.40×10^{-13} cm. However the calculations of Ravenhall¹⁷ on a model very close to the half-uniform and half-Gaussian make computations for this compromise model unnecessary. The shell model calculations of this author favor an rms radius of 2.41×10^{-13} cm and a charge distribution lying close to a half-uniform and half-Gaussian model, in excellent agreement with the calculations reported in this paper. It is to be noted that the experimental shape as well as the absolute values of cross section are in agreement with the theoretical

calculations of this paper and also with those of Ravenhall. The agreement with our calculations is shown in Fig. 11.

We have also carried out calculations at 150 Mev. In this case the Gaussian model again fits excellently with an rms radius of 2.47×10^{-13} cm. The uniform model provides a good fit with an rms radius of 2.31×10^{-13} cm. The data at 150 Mev do not permit as extensive a check as those at 187 Mev and hence are less discriminatory with respect to the uniform charge distribution than the data at the higher energy.

Finally the single point observed at 80 Mev and 90° does not distinguish the type of charge distribution but provides an rms radius of 2.02×10^{-13} cm accompanied by a large experimental error of plus or minus 0.4×10^{-13} cm. Thus the data observed at all energies and angles are consistent with a model lying between a Gaussian charge distribution and a uniform model. An exponential charge distribution is not possible. The best determination of an rms radius provides a value near

$(2.40 \pm 0.25) \times 10^{-13}$ cm. Any error in this figure due to the use of the Born approximation instead of the exact phase shift calculations of Ravenhall and Yennie would amount to less than 1 percent and would make the radius smaller by this amount. It is interesting to examine the equivalent value of r_0 given by this determination, where

$$R = r_0 A^{1/3} \times 10^{-13} \text{ cm}, \quad (3)$$

and R is the usual "radius" (not rms) of the uniformly charged model of the nucleus. r_0 is thus determined to be 1.36 and is larger than the value appropriate to heavier nuclei.^{2,3}

V. ACKNOWLEDGMENTS

We are indebted to Dr. D. G. Ravenhall for many fruitful discussions and also for the communication before publication of the results of his calculations. We also appreciate the assistance of Dr. B. Hahn and Dr. J. A. McIntyre in taking the elastic data at 100° .

Pion Production by Neutrons on Helium*

PETER H. MOULTHROP

Radiation Laboratory, Department of Physics, University of California, Berkeley, California

(Received April 1, 1955)

A helium-filled 36-atmosphere diffusion cloud chamber in a pulsed 21 000-gauss magnetic field was operated in the 300-Mev neutron beam of the 184-inch cyclotron. Two hundred and ninety-five negative pions were found, with associated prongs as indicated in the table.

Reaction	Percent
$n + \alpha \rightarrow \alpha + p + \pi^-$	5.7 ± 1.4
$n + \alpha \rightarrow p + \text{He}^3 + n + \pi^-$	32.0 ± 3.3
$n + \alpha \rightarrow \left\{ \begin{array}{l} \alpha + p + \pi^- \text{ or} \\ p + \text{He}^3 + n + \pi^- \end{array} \right\}$	4.6 ± 1.2
$n + \alpha \rightarrow d + \text{He}^3 + \pi^-$	30.4 ± 3.2
$n + \alpha \rightarrow p + p + d + n + \pi^-$	15.4 ± 2.3
$n + \alpha \rightarrow d + d + p + \pi^-$	6.2 ± 1.5
$n + \alpha \rightarrow t + p + p + \pi^-$	3.3 ± 1.1
$n + \alpha \rightarrow p + p + p + n + n + \pi^-$	1.8 ± 0.8
$n + \alpha \rightarrow \text{unclassified} + \pi^-$	0.6 ± 0.4
Total	100.0

INTRODUCTION

AN experiment has been performed on the production of mesons by 300-Mev neutron bombardment of helium gas contained in a high-pressure diffusion cloud chamber. Considerable advantages are inherent in the cloud chamber method in that a pure target is used, mesons of all angles and energies are detected, and measurements can be made on all prongs coming from a star in which a meson originates. As negative

A comparison is drawn between these results and the cross sections measured by Tannenwald for 90-Mev neutrons on helium. The comparison shows (a) the probability of the alpha particle's being broken up is much larger in the pion-production experiment, indicating the importance of large momentum transfers in pion production, (b) there are many more fast deuterons associated with pion production than pickup deuterons in the 90-Mev experiment, (c) the other inelastic cross sections are in good agreement if the principle of charge symmetry is invoked.

The energy distribution of the mesons is in good agreement with that found in a similar experiment with an oxygen-filled chamber. The angular distribution of the pions is also similar to that obtained by other investigators. Two cases of neutral pion production were detected by the π^0 's decay into an electron pair and one gamma ray. One example of triplet production,

$$\gamma + e^- \rightarrow e^+ + e^- + e^-,$$

was observed.

mesons predominated over positives by a large factor and neutrals can only be detected in rare instances, most of the following is limited to negative mesons. Attention in this experiment was focused on the following points: branching ratios for the various pion-production reactions; fast prongs associated with pion production; angular distribution of the pions; energy distribution of the pions; energy distribution of the neutrons incident in pion-production reactions; the total cross section; infrequent events; and the cloud chamber.

* This work was done under the auspices of the U. S. Atomic Energy Commission.